

## A 290-310 GHz Single Sideband Mixer with Integrated Waveguide Filters

Guo, Cheng; Shang, Xiaobang; Lancaster, Michael J.; Xu, Jun; Powell, Jeffrey; Wang, Hui; Parow-Souchon, Kai; Henry, Manju; Vegas, Colin; Alderman, Byron; Huggard, Peter G.

DOI:

[10.1109/TTHZ.2018.2841771](https://doi.org/10.1109/TTHZ.2018.2841771)

License:

Creative Commons: Attribution (CC BY)

### Document Version

Publisher's PDF, also known as Version of record

### Citation for published version (Harvard):

Guo, C, Shang, X, Lancaster, MJ, Xu, J, Powell, J, Wang, H, Parow-Souchon, K, Henry, M, Vegas, C, Alderman, B & Huggard, PG 2018, 'A 290-310 GHz Single Sideband Mixer with Integrated Waveguide Filters', *IEEE Transactions on Terahertz Science and Technology*, vol. 8, no. 4, pp. 446-454.  
<https://doi.org/10.1109/TTHZ.2018.2841771>

[Link to publication on Research at Birmingham portal](#)

### General rights

Unless a licence is specified above, all rights (including copyright and moral rights) in this document are retained by the authors and/or the copyright holders. The express permission of the copyright holder must be obtained for any use of this material other than for purposes permitted by law.

- Users may freely distribute the URL that is used to identify this publication.
- Users may download and/or print one copy of the publication from the University of Birmingham research portal for the purpose of private study or non-commercial research.
- User may use extracts from the document in line with the concept of 'fair dealing' under the Copyright, Designs and Patents Act 1988 (?)
- Users may not further distribute the material nor use it for the purposes of commercial gain.

Where a licence is displayed above, please note the terms and conditions of the licence govern your use of this document.





When citing, please reference the published version.

### Take down policy

While the University of Birmingham exercises care and attention in making items available there are rare occasions when an item has been uploaded in error or has been deemed to be commercially or otherwise sensitive.

If you believe that this is the case for this document, please contact [UBIRA@lists.bham.ac.uk](mailto:UBIRA@lists.bham.ac.uk) providing details and we will remove access to the work immediately and investigate.

# A 290–310 GHz Single Sideband Mixer With Integrated Waveguide Filters

Cheng Guo , Xiaobang Shang , *Member, IEEE*, Michael J. Lancaster, *Senior Member, IEEE*, Jun Xu, Jeffrey Powell, Hui Wang, Kai Parow-Souchon, Manju Henry , Colin Viegas, Byron Alderman, and Peter G. Huggard , *Senior Member, IEEE*

**Abstract**—A 290–310 GHz Schottky diode based subharmonic mixer with integrated, low loss, impedance matching waveguide cavity filters is presented in this paper. This mixer was designed for use in a 300 GHz communication system with a 20 GHz intermediate frequency band centred at 15 GHz. Image rejection of the 260–280 GHz lower sideband, as well as impedance matching, was achieved using an integrated third-order filter in the RF waveguide. The conventional coupling matrix was used to design the filter even though the impedance presented to the RF port was complex and frequency dependent. The mixer was measured to have: 1) single sideband conversion loss of 9–10 dB across the upper sideband, with a mixer noise temperature of 2000–2600 K; 2) a return loss at the RF port better than 12 dB, with three filter reflection zeroes (poles) distinguishable; and 3) a sideband rejection ratio from 13 to 25 dB, demonstrating the RF filter’s excellent performance in terms of impedance matching and filtering.

**Index Terms**—Image rejection, planar Schottky diode, subharmonic mixer, waveguide filters.

## I. INTRODUCTION

THERE is a need for Schottky diode based mixers, operating at submillimeter-wave frequencies for diverse applications. Examples include planetary and earth observations [1]–[3], high-resolution THz imaging and radar [4]–[6], and

Manuscript received February 5, 2018; revised April 16, 2018; accepted May 15, 2018. Date of publication June 1, 2018; date of current version July 2, 2018. This work was supported by the U.K. Engineering and Physical Science Research Council (EPSRC) under Contract EP/M016269/1. (*Corresponding author: Cheng Guo.*)

C. Guo and M. J. Lancaster are with the Department of Electronic, Electrical, and Systems Engineering, University of Birmingham, Birmingham B15 2TT, U.K. (e-mail: spmguo@163.com; m.j.lancaster@bham.ac.uk).

X. Shang was with the Department of Electronic, Electrical and Systems Engineering, University of Birmingham, Birmingham B15 2TT, U.K. He is now with the National Physical Laboratory, Teddington TW11 0LW, U.K. (e-mail: shangxiaobang@gmail.com).

J. Xu is with the School of Physical Electronics, University of Electronic Science and Technology of China, Chengdu 610054, China (e-mail: xujun@uestc.edu.com).

J. Powell is with Skyarna Ltd., Halesowan, West Midlands B63 3TT, U.K. (e-mail: jeff.powell@skyarna.com).

H. Wang, K. Parow-Souchon, M. Henry, B. Alderman, and P. G. Huggard are with the Department of Space Science and Technology, Rutherford Appleton Laboratory, Oxfordshire OX11 0QX, U.K. (e-mail: hui.wang@stfc.ac.uk; kai.parow-souchon@stfc.ac.uk; manju.henry@stfc.ac.uk; byron.alderman@stfc.ac.uk; peter.huggard@stfc.ac.uk).

C. Viegas is with the Millimetre Wave Technology Group, Rutherford Appleton Laboratory, Oxfordshire OX11 0QX, U.K., and also with Teratech Components, Oxfordshire OX11 0QX, U.K. (e-mail: colin.vegas@stfc.ac.uk).

Color versions of one or more of the figures in this paper are available online at <http://ieeexplore.ieee.org>.

Digital Object Identifier 10.1109/TTHZ.2018.2841771

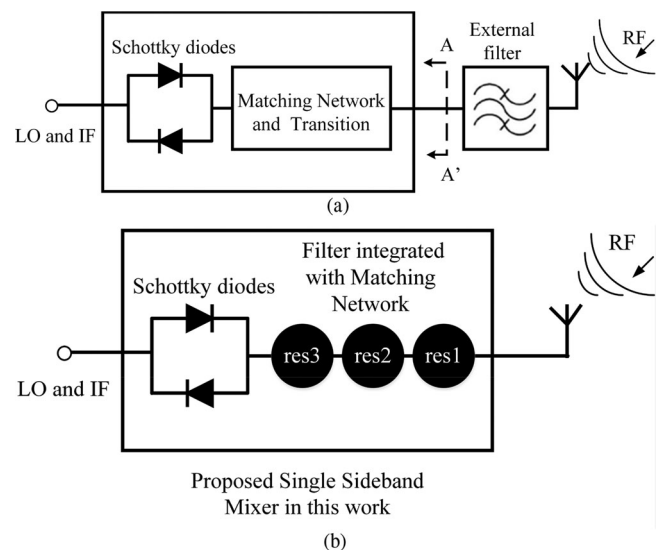


Fig. 1. Illustration diagrams of two different configurations of mixers for single-sideband operation. (a) Conventional DSB mixer with external waveguide or FSS bandpass filter. (b) Mixer with integrated waveguide resonator based bandpass filter.

multi-Gbps THz communication [7]–[9]. Heterodyne mixers usually exhibit double-sideband (DSB) operation, i.e., signals from lower sideband (LSB) and upper sideband (USB) are simultaneously converted to the intermediate frequency (IF) [9]–[12]. However, in many cases (e.g., using closely spaced channels for THz communications, and some earth observations), only one of the sidebands is of interest, and rejection of the unwanted sideband is required. External filters can be used to provide single sideband (SSB) detection. A typical configuration is shown in Fig. 1(a), where the DSB mixer and an external bandpass filter (BPF) are cascaded to provide SSB operation. Filters at submillimeter-wave frequencies are often quasi-optical frequency selective surfaces (FSS) or waveguide cavity filters due to their low-loss properties [13]–[15]. For example, an FSS was produced for an airborne limb-sounding instrument [13], where the measured insertion loss is 0.6 dB across the LSB (316.5–325.5 GHz) while the rejection over the USB (349.5–358.5 GHz) is greater than 30 dB. Waveguide filters are also reported to have low loss performance [14]–[16]. Compared with the quasi-optical filters, waveguide filters are much more compact and they are usually preferred in THz communication systems [7]–[9].

For a conventional DSB mixer, the Schottky diodes are impedance matched on the microstrip circuit, and a microstrip to waveguide transition is used. Where sideband rejection is needed, then the mixer component can be preceded by a waveguide or quasi-optical filter, as exhibited in Fig. 1(a).

A novel alternative approach, explored by us in this paper, is to impedance match the diodes directly using the waveguide filter, with the last resonator in the filter directly coupled to the input of the diodes, as shown in Fig. 1(b). Moving the filter toward the diodes eliminates one of the microstrip matching stages, shortens waveguides thereby reducing loss, and makes the structure much more compact. It also eliminates potential mismatches between the waveguide flanges and impedance mismatches between the mixer and the external filter along line A-A' in Fig. 1(a).

The concept of filter matching has been used previously, and filters with complex load impedance was discussed in [20]. It was demonstrated, using low-frequency power amplifiers, that filters can be used to perform filtering and complex impedance matching by tuning the coupling between the resonators and by changing the dimensions of the resonators to alter their centre frequencies [21], [22].

In this paper, we describe the application of similar principles for a Schottky diode based SSB mixer. Image rejection over the 260–280 GHz LSB and impedance matching are achieved simultaneously using a third-order waveguide cavity filter. The layout of the device is shown in Fig. 2(a). Compared with the conventional approach shown in Fig. 1(a), this integrated design leads to a reduced circuit complexity, a smaller size, and a reduced loss. To the best of the author's knowledge, this is the first time that filters have been used to impedance match any device at a submillimeter-wave frequency in the open literature.

Filters are not the only solution to achieve sideband rejection. For example, image rejection mixers or sideband separating mixers do not require an RF filter [18], [19]. To achieve this, two identical DSB mixers were combined using hybrid networks [17] at the RF and IF ports: the LSB and USB channels can then be separated. Rather than rejecting the unwanted sideband, this technology down converts both into distinct IF channels. However, the system complexity was significantly increased (component numbers were doubled and a power dividing network was needed for the LO port) and the losses from the hybrid networks cannot be neglected. The sideband rejection approach proposed by us gives a comparable performance in terms of sideband rejection ratio (SBR) and conversion losses, however, it has much simpler design and offers easier fabrication.

## II. DESIGN OF THE MIXER

The mixer uses a split-block waveguide design using standard WR-5 and WR-3 waveguides for the LO and RF ports. The IF output is connected to an SMA connector via a microstrip RF blocking filter. This is shown in the enlarged view of the mixer in Fig. 2(b), with the whole mixer structure shown in Fig. 2(a), with input and output filters comprising resonators 1–6. The antiparallel Schottky diode chip is soldered to a thin film quartz substrate, and coupled to the third and sixth resonators via E-plane probes directly. The E-plane probes effec-

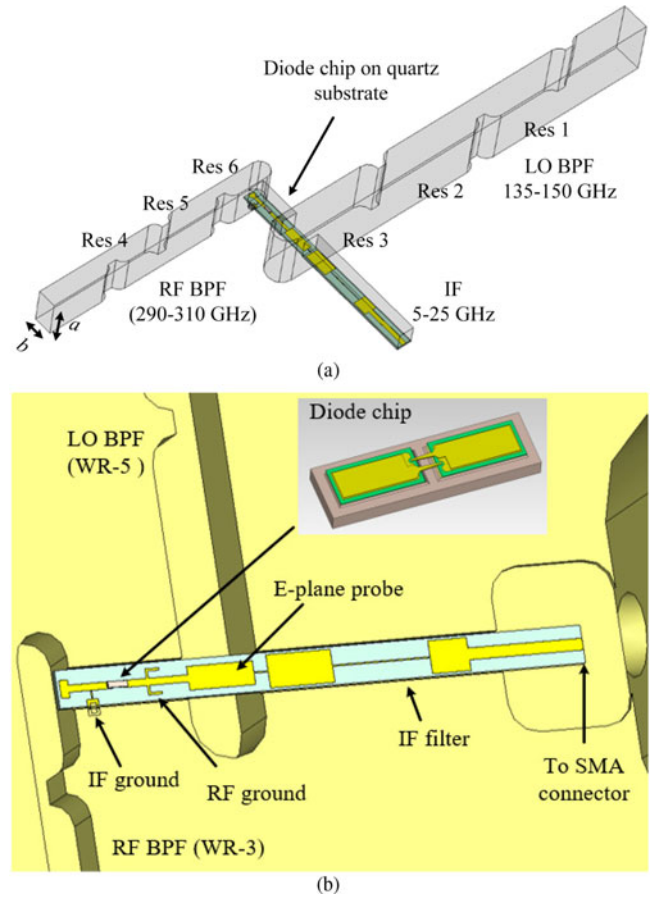


Fig. 2. Proposed image rejection mixer using integrated waveguide filters. (a) 3-D model of the mixer.  $a = 0.864$  mm,  $b = 0.432$  mm. (b) Enlarged view of the mixer, the Schottky diode chip used in this work is Teratech part # AP1, which contains 2 antiparallel anodes, each of  $9.5 \times 10^{-12}$  m<sup>2</sup> anode area. The parameters are: series dc resistance  $R_s = 13 \Omega$ , ideality factor  $n = 1.2$ , saturation current  $I_s = 1.5$  fA and the nonlinear junction capacitance at zero bias voltage  $C_{j0} = 1.44$  fF.

tively become part of the resonators and allow coupling to the microstrip circuit containing the diodes. Altering the geometry of the probe varies the external coupling factor ( $Q_e$ ) [23] to the microstrip, providing one of the inherent design parameters of the filter. This allows the structures on the microstrip circuit be effective, simple and compact.

To design the filters that directly impedance match the diode chip, the following three step approach is applied:

- 1) The mixer together with matching filters, see Fig. 2(a), is separated into three parts: 1) the diode chip and its waveguide housing, 2) the LO and IF filter, and 3) the RF filter, as shown in Fig. 3. A three-dimensional (3-D) model of the Schottky diode chip must also be modeled accurately by full-wave simulators; this is critical for the mixer design [24].
- 2) The frequency dependent embedding impedances of the diode chip [Teratech AP1/G2/0p95, see Fig. 2(b)], with its waveguide housing at each operating frequency, namely,  $Z_{RF}$ ,  $Z_{LO}$ , and  $Z_{IF}$  need to be extracted for the filter design. Circuit simulation software, such as ADS [25], is used to model the nonlinear Schottky junction and to apply harmonic balance simulation to this structure. The

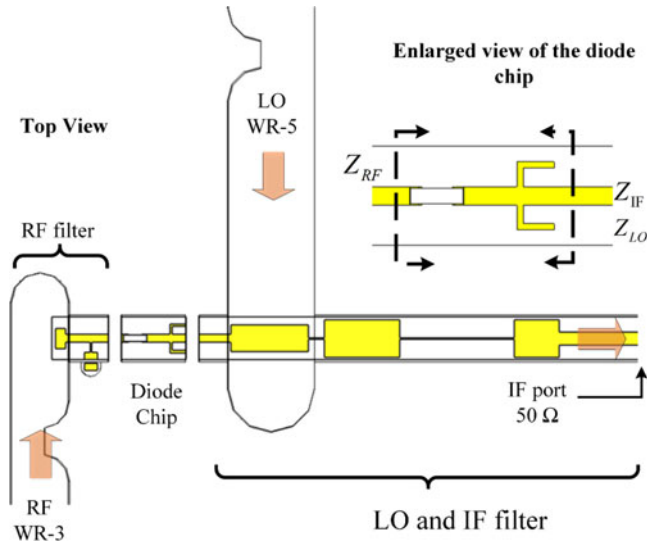


Fig. 3. Mixer model is separated into three parts. Impedances extracted from the diode chip can be used to design the filters.

TABLE I  
PORT IMPEDANCES OF THE SINGLE ANODE AND THE DIODE CHIP

	Single anode	Diode chip *
$Z_{RF}$ @ 300 GHz	157-j58 $\Omega$	36+j32 $\Omega$
$Z_{LO}$ @ 142.5 GHz	342-j237 $\Omega$	57+j51 $\Omega$
$Z_{IF}$ @ 15GHz	158-j44 $\Omega$	75-j34 $\Omega$

\*CHIP IMPEDANCE INCLUDING THE WAVEGUIDE HOUSING AND RF GROUND BETWEEN REFERENCE PLANE A-A' AND B-B' SHOWN IN FIG.3. THE LO INPUT POWER IS 2MW.

impedances can be extracted by optimizing the complex port impedances at each harmonic. An open circuit is presented for nontuned harmonics. The driving power at the LO port is also optimized. The goals are set to minimize the mixer conversion loss and LO/RF return losses. The extracted impedances for a single Schottky anode and the diode chip are given in Table I, under the optimized LO power of 2 mW. These complex impedances are frequency and power dependent: this will be discussed in some detail later.

- 3) The RF and LO filters are designed to match the complex impedances obtained from Step 2 directly. The complex impedance can be taken into account in the coupling matrix by adjusting the coupling coefficients (i.e., for self-coupling and external coupling) of the resonator that is connected to the complex load [20]. This approach needs prior knowledge of the complex impedance presented to the affected resonator [20]. In our work, extracting the exact value of the complex impedance presented to the cavity resonator is not straightforward, due to the fact that two different transmission lines (waveguide and microstrip) were involved. Therefore, an alternative approach is utilized here for the design of the filters, as discussed below.

#### A. LO and IF Filter Design

The filter has one waveguide port and two microstrip ports, as shown in Fig. 4. Port 1 is physically connected to the diode

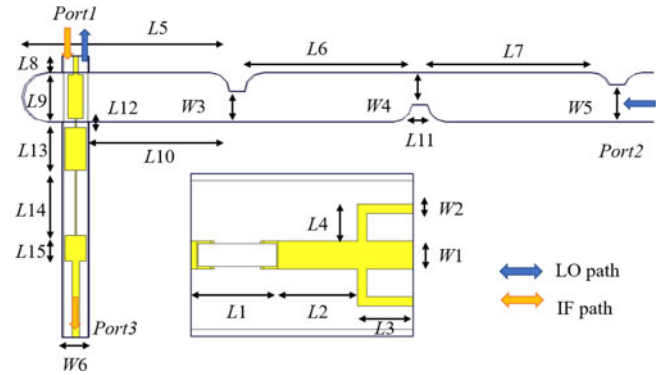


Fig. 4. Design of the LO and IF filter. Dimensions are (in millimeters):  $L_1 = 0.188$ ,  $L_2 = 0.172$ ,  $L_3 = 0.120$ ,  $L_4 = 0.080$ ,  $L_5 = 2.723$ ,  $L_6 = 2.206$ ,  $L_7 = 2.397$ ,  $L_8 = 0.239$ ,  $L_9 = 0.575$ ,  $L_{10} = 1.849$ ,  $L_{11} = 0.200$ ,  $L_{12} = 0.123$ ,  $L_{13} = 0.563$ ,  $L_{14} = 0.854$ ,  $L_{15} = 0.338$ ,  $W_1 = 0.060$ ,  $W_2 = 0.020$ ,  $W_3 = 0.400$ ,  $W_4 = 0.420$ ,  $W_5 = 0.488$ ,  $W_6 = 0.350$ .

chip, hence the complex and frequency dependent impedances presented to it are  $Z_{LO}$  and  $Z_{IF}$ . The impedances of ports 2 and 3 are real. A third-order Chebyshev filter with a 15 dB passband return loss and a bandwidth of 15 GHz centred at 142.5 GHz is designed to match  $Z_{LO}$ . It consists of three waveguide resonators where the third resonator is coupled to the diode chip through an E-plane probe. Here we consider the LO path only and regard it as a two-port filter, since the IF filter blocks the signal from the LO waveguide and behaves effectively like an open circuit.

The design procedure described in [23] is used to design the filter. The resulting nonzero elements of the coupling matrix (coupling coefficients ( $m_{ij}$ ) and external couplings ( $Q_e$ ) are:  $m_{12} = m_{23} = 0.093$ , and  $Q_{e1} = Q_{e3} = 10.54$ . Note that this is a matrix developed for real loads. The fact that the impedance is complex can be considered during the full wave simulations. As discussed in [20], the impact of the complex load can be compensated by adjusting its adjacent resonator [i.e., resonator 3 in this case, see Fig. 1(a)]. Resonator 3 together with the probe is now treated as a single component, which operates effectively in the same way as a resonator terminated with real loads. In other words, the conventional coupling matrix can be used for the filter design. Additionally, considering the impedance,  $Z_{LO}$ , presented to the port varies with frequency; it can be written into a file and assigned to the port in full wave simulators, such as CST [26].

The filter is then optimized as a conventional filter, tuning the initial dimensions obtained from the coupling matrix for the LO path. For the IF path, the  $S_{11}$  below 25 GHz and  $S_{31}$  at 135–150 GHz are minimized by optimizing the dimensions marked as  $L_{12} - L_{15}$ . The optimized dimensions are given in Fig. 4, along with some physical dimensions of the diode chip. The optimized filter performance is shown in Fig. 5. The simulated  $S_{11}$  for the LO path is below  $-15$  dB for 135–150 GHz, the isolation between ports 1 and 3 is better than 12 dB. For the IF path, the  $S_{11}$  is better than  $-10$  dB for 0–25 GHz.

#### B. RF Filter Design

A third-order Chebyshev filter with a 15 dB passband return loss and a bandwidth of 20 GHz centred at 300 GHz is similarly



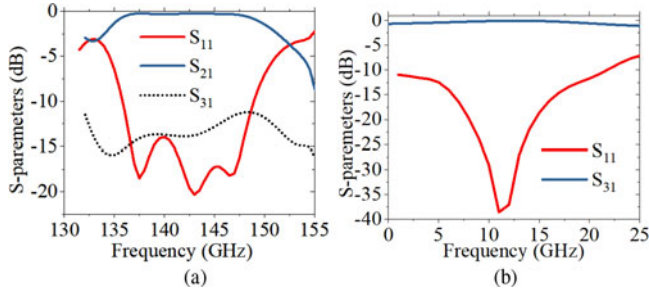


Fig. 5. S-parameter simulation results of the filter for (a) LO channel and (b) IF channel.

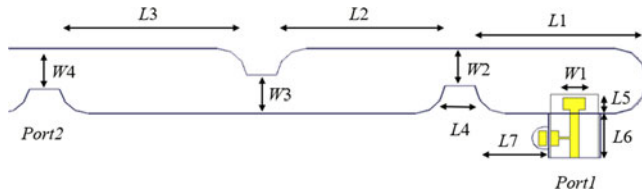


Fig. 6. Design of the RF filter. Dimensions are (in millimeters):  $L_1 = 1.160$ ,  $L_2 = 1.135$ ,  $L_3 = 1.260$ ,  $L_4 = 0.200$ ,  $L_5 = 0.200$ ,  $L_6 = 0.320$ ,  $L_7 = 0.494$ ,  $W_1 = 0.150$ ,  $W_2 = 0.250$ ,  $W_3 = 0.254$ ,  $W_4 = 0.272$ .

designed to match  $Z_{RF}$ . The resulting nonzero elements of the coupling matrix and  $Q_e$  values are:  $m_{12} = m_{23} = 0.059$  and  $Q_{e1} = Q_{e3} = 16.65$ . The resulting starting values for the filter dimensions are optimized in CST using the frequency dependent  $Z_{RF}$ . Optimized filter dimensions are shown Fig. 6: the filter performance will be presented in Section IV.

### C. Mixer Design

S-parameter files of the filters and the diode chip are exported from CST to ADS and reconstructed schematically. Harmonic balance simulation is applied to the mixer circuit to predict the performance. The simulated performance of the mixer can be summarized as follows: LO return loss better than 15 dB from 135–150 GHz, maximum RF return loss of around 15 dB from 290–310 GHz, IF return loss better than 10 dB from 1–25 GHz, SSB conversion loss of around 8 dB and SBR at the 260–280 GHz band from 13 to 20 dB under 2–2.5 mW LO driving power. To avoid repetition, predicted performance data is included in the measurement result graphs presented later.

## III. FABRICATION, ASSEMBLY, AND Y-FACTOR MEASUREMENT OF THE MIXER

The split-block waveguide parts of the mixer were CNC machined from brass and then gold electroplated. The substrate for the microstrip circuit is 50  $\mu\text{m}$  thick fused quartz with the diode chip fixed to the microstrip by soldering. Fig. 7 shows a photograph of the bottom half of the device.

The mixer performance in terms of conversion loss and noise temperature was characterized using the Y-factor method [24]. The mixer LO was driven by a 135–150 GHz frequency multiplied source with a maximum output power of 3 mW, as calibrated by an Erickson PM4 waveguide power meter. A feed-

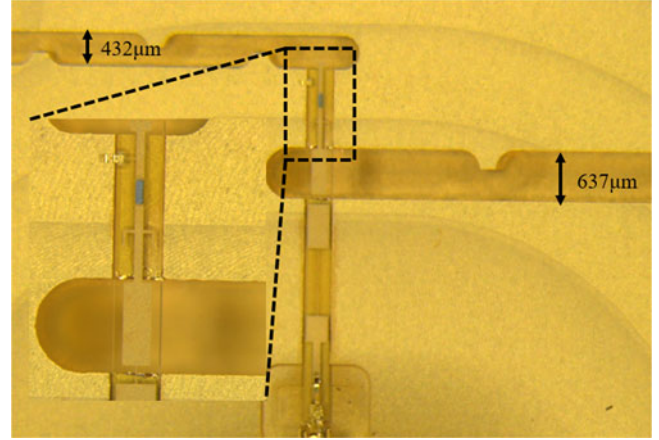


Fig. 7. Photograph of the bottom half of the mixer, with the quartz circuit containing the Schottky diode chip installed.

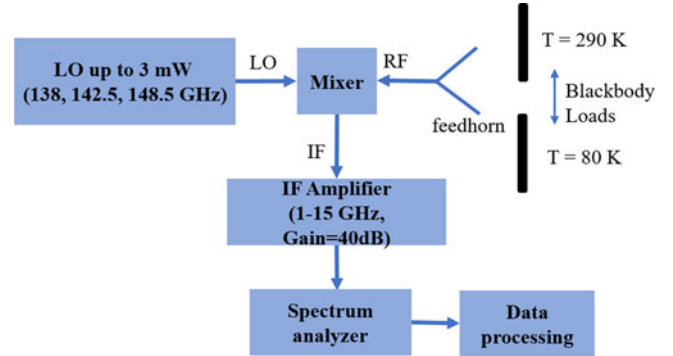


Fig. 8. Y-factor measurement setup.

horn antenna coupled the radiation alternatively from a room temperature load (290 K) and a liquid nitrogen cooled black body (77 K) into the RF port of the mixer. As the power radiated by the black body load was low, the mixer's IF output was amplified by 40 dB using a 1–15 GHz low noise, two stages amplifier chain. The output from this was monitored by a Rohde & Schwarz ROH-FSU-05 spectrum analyser, as shown in Fig. 8. The conversion loss and noise temperature of the mixer can be computed from the measurements [24].

The designed 15 dB return loss bandwidth of the RF filter is 290–310 GHz. However, the available amplifier chain at hand operates over 1–15 GHz, covering only part of the 20 GHz working bandwidth of the mixer. To address this, three different setups were used to cover the overall RF bandwidth. The corresponding LO frequencies,  $2 \times \text{LO} = 276 \text{ GHz}$ ,  $2 \times \text{LO} = 285 \text{ GHz}$ , and  $2 \times \text{LO} = 297 \text{ GHz}$ , and associated LSB and USB, are shown in Fig. 9. The combination covered the RF from 277 to 312 GHz. Due to the existence of the RF filter, although the Y-factor method itself measured the DSB mixer performance, results from Fig. 9(a) and (b) actually correspond to the behavior of a SSB mixer. This is demonstrated in Fig. 10, where the measured performances of the mixer at different LO power and frequencies are plotted. The two conversion loss curves are for the mixer working at SSB

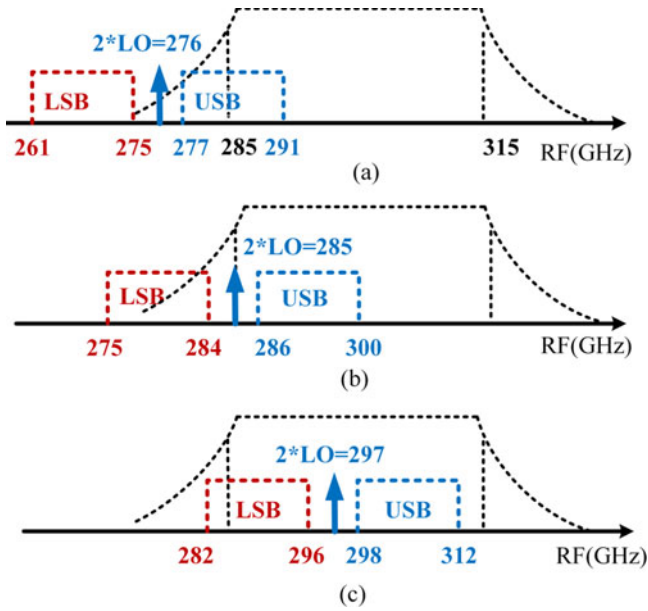


Fig. 9. Measurement of the mixer using three LO frequencies. The  $-15$  dB return loss bandwidth of the RF filter is  $290\text{--}310$  GHz while the equivalent  $-3$  dB bandwidth of the same filter is  $285\text{--}315$  GHz: black dashed curve. (a) SSB characterization with  $2 \times \text{LO} = 276$  GHz. (b) Same with  $2 \times \text{LO} = 285$  GHz. (c) DSB operation with  $2 \times \text{LO} = 297$  GHz.

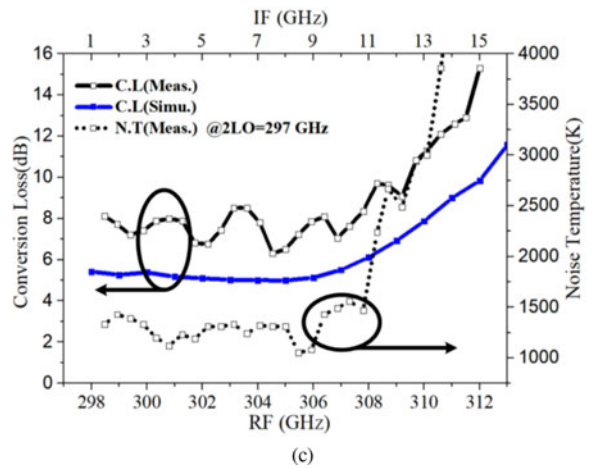
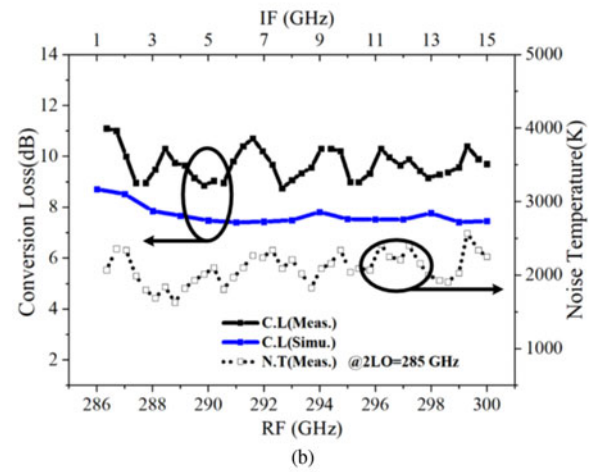
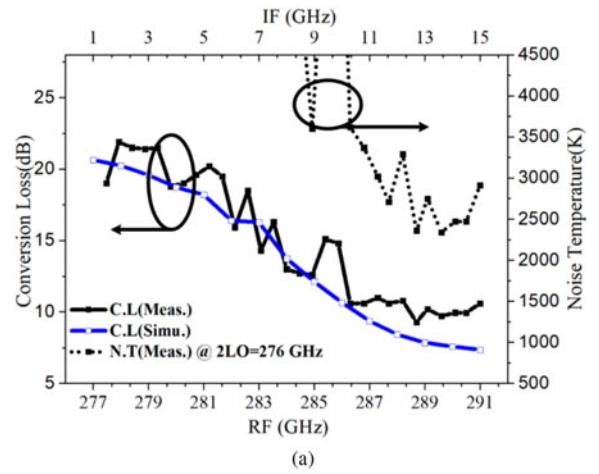


Fig. 11. Simulated and measured mixer conversion losses and noise temperatures. (a)  $2 \times \text{LO} = 276$  GHz (SSB operation). (b)  $2 \times \text{LO} = 285$  GHz (SSB operation). (c)  $2 \times \text{LO} = 297$  GHz (DSB operation).

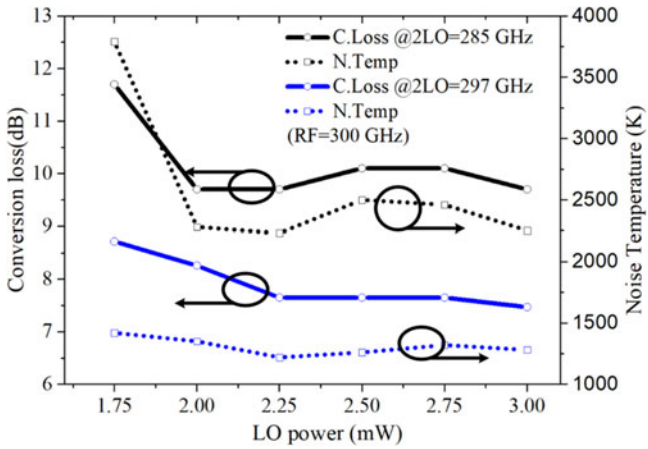


Fig. 10. Measured conversion loss and noise temperature performance of the mixer under different LO power levels for  $2 \times \text{LO} = 285$  and  $297$  GHz. At a single point  $\text{RF} = 300$  GHz.

operation, with  $2 \times \text{LO} = 285$  GHz; and for DSB operation, with  $2 \times \text{LO} = 297$  GHz (while the RF was fixed at  $300$  GHz). A difference of  $\sim 2.5$  dB in conversion loss is found in Fig. 10, in good agreement with the theoretical difference between SSB and DSB of  $3$  dB [24]. From this we also know the optimum LO input power was at  $2.5\text{--}3$  mW.

The measured RF, and hence IF, dependences of conversion loss and noise temperatures for the three LO frequencies with  $2.5$  mW input LO power are shown in Fig. 11. Fig 11(b) shows that for  $2 \times \text{LO} = 285$  GHz, the obtained SSB conversion loss ripples from  $9\text{--}11$  dB and the noise temperature is around  $2000\text{--}2600$  K. The conversion loss is typically  $2$  dB higher

than predicted. On the other hand, as shown in Figs. 9(c) and 11(c), under the condition of  $2 \times \text{LO} = 297$  GHz, the mixer was in DSB operation and the measured conversion loss is from  $6\text{--}8$  dB with  $1000\text{--}1500$  K noise temperature. Again, predicted conversion loss is about  $2$  dB lower but there is a good agreement between the curve trends. The  $2$  dB loss difference was mainly due to the RF resistance of the diode being higher than

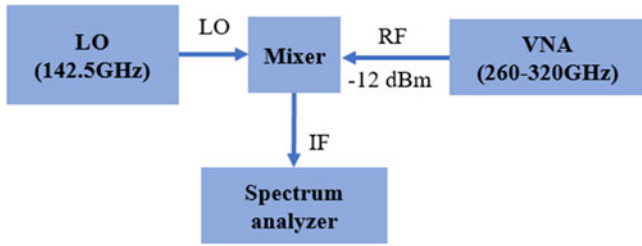


Fig. 12. RF return loss and SBR measurement setup.

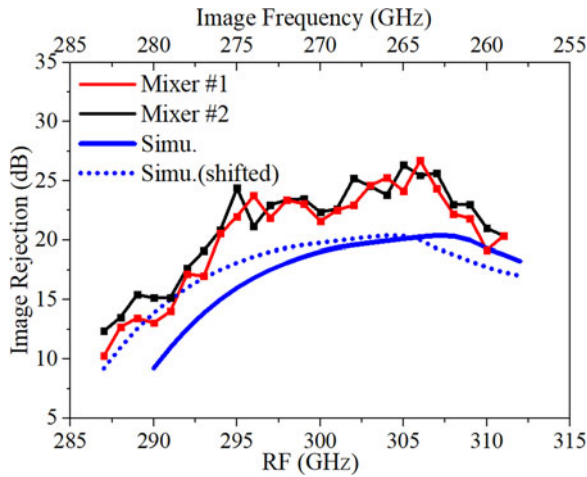


Fig. 13. Simulated and measured image rejection of the mixer. When the measured return loss of the RF port is accounted for, as described in the text, the predicted SBR shifts to the blue dotted curve.

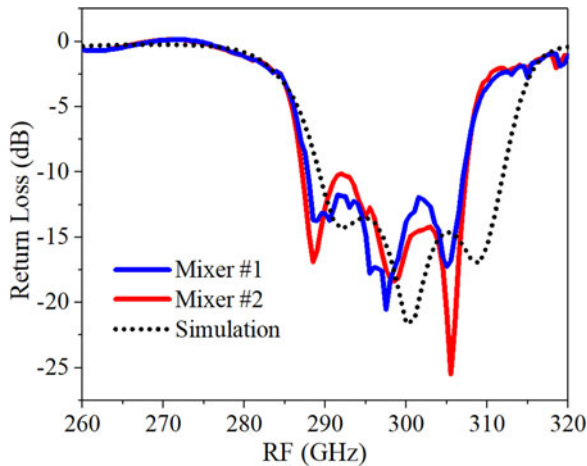


Fig. 14. Simulated and measured RF return losses for two mixers. A frequency redshift of approximately 3 GHz can be observed with respect to predictions.

the measured dc resistance at such frequency band [27]. Also, the ripples in the measured curves in Fig. 11 may result in the mismatches between the IF port and the cascading amplifiers.

From Fig. 11(a), with  $LO = 2 \times 276$  GHz, the SSB conversion loss at 277–280 GHz is around 19–22 dB, which is 10–13 dB higher than the typical SSB conversion loss within the 290–310 GHz band, as shown in Fig. 11(b). Also, it can be

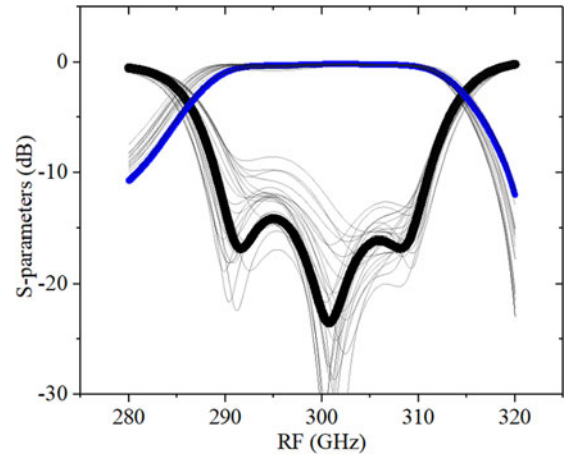


Fig. 15. Tolerance analysis of the matching filter.

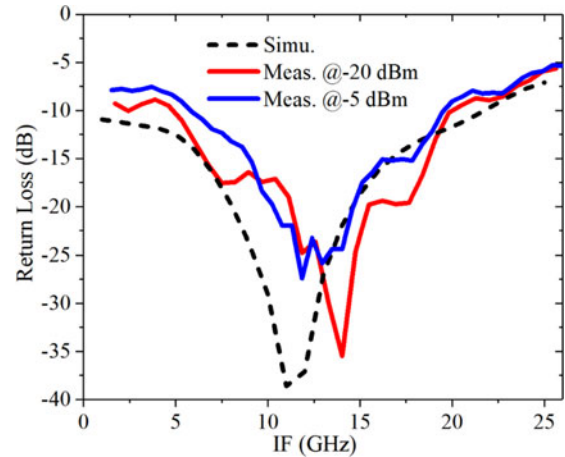


Fig. 16. Simulated and measured mixer IF return loss at two different input power levels for mixer #1. The response of the other mixer is similar.

noticed from Fig. 11(c) that the conversion loss starts to increase from 307 GHz, this is due to the existence of the RF filter and the trends agrees well with simulations.

Due to the limitations from the IF amplifier bandwidth and the LO source tuning range, the performance of the mixer for RF below 277 GHz could not be characterized by the Y-factor method. In the next section, we present results on the mixer SBR and the RF return loss characterization using a VNA, over the whole RF range.

#### IV. MEASUREMENT OF RETURN LOSS AND SBR

A Keysight VNA with the VDI frequency extender was used to measure the RF return loss and the sideband ratio simultaneously. The VNA was connected to the RF port of the mixer: the extender had a nominal  $-12$  dBm output power from 260 to 320 GHz. The LO port of the mixer was driven by a source with  $2 \times LO = 285$  GHz. Since the power from the VNA was much higher than the blackbody radiation so the down-converted signal can be directly read by the spectrum analyser. This is shown in Fig. 12. In this measurement, we were not interested in the absolute value of the conversion loss across the two



TABLE II  
COMPARISON OF SOME SCHOTTKY DIODE BASED SUBHARMONIC MIXERS WORKING AT 300 GHz BAND

Ref	Mixer type	RF (GHz)	Conversion Loss (dB)	Mixer noise temperature (K)	Image Rejection (dB)
[7]	DSB mixer with external filter	305-345	9-11 (SSB, Mixer only) >1.41 (External filter loss)	900-1100K (DSB)	> 30 @325 GHz
[10]	DSB mixer	300-360	6-7 (DSB)	1050-1270K (DSB)	N.A
[18]	2SB mixer	320-360	10-11 (SSB)	N.A	7.2-24.1
[19]	2SB mixer	320-360	9 (SSB)	900 (DSB) 3000 (SSB)*	>15
This work	DSB mixer with integrated filter	290-310	6-8 (DSB) 9-10 (SSB)	1000-1500K (DSB) 2000-2600 K (SSB)	13-25 @260-280 GHz

\*Including an integrated IF LNA.

sidebands, but the difference between the two. This is the reason only a ratio measurement was performed as detailed above, this allows us to eliminate the calibration of the IF channel, but the output power from the VNA must be carefully calibrated. This was done by measuring the output power of the VNA using an Erickson PM4 waveguide power meter and changing the output power of the VNA to get a constant reading over the frequency band. Fig. 13 shows the simulated and measured SBRs for two fabricated mixers, called mixer #1 and mixer #2. The measurement results were obtained by subtracting the received IF power with the RF input corresponding to USB and LSB, so the losses from the IF channel were cancelled. The obtained sideband ratio (image rejection) was in the range 13–25 dB. This agreed with the results from Section III where the SBR at 277–280 GHz was 10–13 dB (mixer #1).

The RF return loss value can be directly obtained from the VNA and the results are shown in Fig. 14. Excellent agreement is obtained between the two devices. The simulated RF return loss is around 15 dB from 290–310 GHz and the measured maximum return loss is around 12 dB in the band 287–308 GHz. A frequency shift of about 3 GHz can be observed, approximately 1% of the centre frequency. The effect of this shift on the predicted SBR is indicated in Fig. 13 by the blue dotted line. The return loss measurement results demonstrate the filter was working well in terms of filtering and impedance matching. On the other hand, good image rejection was achieved by using a third-order waveguide filter. The performance can be further improved by increasing the order of the filter or adding transmission zeros if necessary.

Also as we consider filtering, impedance matching and transition which are all realized in the resonators, hence their fabrication tolerances have a direct influence on the performance of the mixer. Fig. 15 shows several results obtained by changing the filter dimensions for  $\pm 10 \mu\text{m}$  (about 1%–2% of the nominal values [16]) of each dimensions. It is also observed in the simulation that the filter response is more sensitive to the position of the E-plane probe rather than the dimensions of the resonator cavities.

The impedance matching of the IF port was also characterized using a Keysight VNA. A 1–25 GHz signal at two different power levels;  $-20 \text{ dBm}$  and  $-5 \text{ dBm}$ , was applied to the IF

port. The simulated and measured results are shown in Fig. 16. The measured responses agreed well with the simulation.

The results obtained in this work are compared to other mixers working at the same frequency band in Table II. The mixer performance in terms of image rejection is similar to that reported by using much more complex two channel image rejection mixers [18], [19]. The SSB conversion loss of this work is similar to the work presented in [7], where the latter requires an additional filter and this brings more loss.

## V. CONCLUSION

A Schottky diode based 300 GHz SSB mixer with integrated waveguide filters is presented. The design approach presented in this paper differs from the conventional approach where the diodes are coupled to the output waveguide, and followed by an external filter. Instead, we provide a new approach where the diode chip is directly coupled to the resonators of waveguide filters via E-plane probes and impedance matched using the RF/LO waveguide filters. This novel integrated design leads to a reduced circuit complexity, smaller size, and lower loss due to the reduced number of individual components and joints/connections.

Simulations of the device predict a SSB conversion loss of 8 dB, while the measured conversion loss at a 2–2.5 mW LO power level was around 9–10 dB with 2000–2600 K noise temperature. The use of the waveguide filter as the RF matching network brings intrinsic image rejection to the mixer with the measured image rejection from 13 to 25 dB for the 260–280 GHz band. Return loss of better than 12 dB was recorded at the RF port and all the reflection zeros (poles) were distinct. The measurement results showed the filters were working well in terms of impedance matching and filtering.

## REFERENCES

- [1] J. Treuttl *et al.*, "A 520–620-GHz Schottky receiver front-end for planetary science and remote sensing with 1070 K–1500 K DSB noise temperature at room temperature," *IEEE Trans. THz Sci. Technol.*, vol. 6, no. 1, pp. 148–155, Jan. 2015.
- [2] E. Schlecht *et al.*, "Schottky diode based 1.2 THz receivers operating at room-temperature and below for planetary atmospheric sounding," *IEEE Trans. THz Sci. Technol.*, vol. 4, no. 6, pp. 661–669, Nov. 2014.



- [3] B. Thomas *et al.*, “Integrated heterodyne receivers for MM & subMM atmospheric remote sensing,” in *Proc. Inst. Eng. Millimeter Wave Products Technol. Technol. Seminar*, 2006, pp. 13–18.
- [4] J. Grajal *et al.*, “Compact radar front-end for an imaging radar at 300 GHz,” *IEEE Trans. THz Sci. Technol.*, vol. 7, no. 3, pp. 268–273, May 2017.
- [5] K. B. Cooper and G. Chattopadhyay, “Submillimeter-wave radar: Solid-state system design and applications,” *IEEE Microw. Mag.*, vol. 15, no. 7, pp. 51–67, Nov./Dec. 2014.
- [6] T. Bryllert, V. Drakinskiy, K. B. Cooper, and J. Stake, “Integrated 200–240-GHz FMCW radar transceiver module,” *IEEE Trans. Microw. Theory Techn.*, vol. 61, no. 10, pp. 3808–3815, Oct. 2013.
- [7] C. Wang *et al.*, “0.34-THz wireless link based on high-order modulation for future wireless local area network applications,” *IEEE Trans. THz Sci. Technol.*, vol. 4, no. 1, pp. 75–85, Jan. 2014.
- [8] T.J. Chung and W.H. Lee, “10-Gbit/s wireless communication system at 300 GHz,” *ETRI J.*, vol. 35, pp. 386–396, Jun. 2013.
- [9] Z. Chen *et al.*, “220 GHz outdoor wireless communication system based on a Schottky-diode transceiver,” *IEICE Electron. Express*, vol. 13, no. 9, 2016, Art. no. 20160282.
- [10] B. Thomas, A. Maestrini, and G. Beaudin, “A low-noise Fixed-tuned 300-360-GHz sub-harmonic mixer using planar Schottky diodes,” *IEEE Microw. Compon. Lett.*, vol. 15, no. 12, pp. 865–867, Dec. 2005.
- [11] P. J. Sobis, N. Wadefalk, A. Emrich, and J. Stake, “A broadband, low noise, integrated 340 GHz Schottky diode receiver,” *IEEE Microw. Compon. Lett.*, vol. 22, no. 7, pp. 366–368, Jul. 2012.
- [12] A. Maestrini *et al.*, “Schottky diode based terahertz frequency multipliers and mixers,” *Comptes Rendus de l’Acad. Sci. Phys.*, vol. 11, no. 7–8, pp. 480–495, Aug.–Oct. 2010.
- [13] R. Dickie *et al.*, “Submillimeter wave frequency selective surface with polarization independent spectral responses,” *IEEE Trans. Antennas Propag.*, vol. 57, no. 7, pp. 1985–1994, Jul. 2009.
- [14] J. Q. Ding *et al.*, “WR-3 band quasi-elliptical waveguide filters using higher order mode resonances,” *IEEE Trans. THz Sci. Technol.*, vol. 7, no. 3, pp. 302–309, May 2017.
- [15] Q. Chen, X. Shang, Y. Tian, J. Xu, and M. J. Lancaster, “SU-8 micro-machined WR-3 band waveguide bandpass filter with low insertion loss,” *Electron. Lett.*, vol. 49, no. 7, pp. 480–482, Mar. 2013.
- [16] H. Yang *et al.*, “WR-3 waveguide bandpass filters fabricated using high precision CNC machining and SU-8 photoresist technology,” *IEEE Trans. THz Sci. Technol.*, vol. 8, no. 1, pp. 100–107, Jan. 2018.
- [17] P. Sobis, J. Stake, and A. Emrich, “A 170 GHz 45 degree hybrid for submillimeter wave sideband separating subharmonic mixers,” *IEEE Microw. Wireless Compon. Lett.*, vol. 18, no. 10, pp. 680–682, Oct. 2008.
- [18] B. Thomas, S. Rea, B. Moyna, B. Alderman, and D. Matheson, “A 320–360 GHz subharmonically pumped image rejection mixer using planar Schottky diodes,” *IEEE Microw. Compon. Lett.*, vol. 19, no. 2, pp. 101–103, Feb. 2009.
- [19] P. J. Sobis, A. Emrich, and J. Stake, “A low VSWR 2SB Schottky receiver,” *IEEE Trans. THz Sci. Technol.*, vol. 1, no. 2, pp. 403–411, Nov. 2011.
- [20] K. Wu and W. Meng, “A direct synthesis approach for microwave filters with a complex load and its application to direct diplexer design,” *IEEE Trans. Microw. Theory Techn.*, vol. 55, no. 5, pp. 1010–1017, May 2007.
- [21] L. Gao, X. Y. Zhang, S. Chen, and Q. Xue, “Compact power amplifier with bandpass response and high efficiency,” *IEEE Microw. Wireless Compon. Lett.*, vol. 24, no. 10, pp. 707–709, Oct. 2014.
- [22] Q. Y. Guo, X. Y. Zhang, J. X. Xu, Y. C. Li, and Q. Xue, “Bandpass class-F power amplifier based on multifunction hybrid cavity–microstrip filter,” *IEEE Trans. Circuits Syst. II, Exp. Briefs*, vol. 64, no. 7, pp. 742–746, Jul. 2017.
- [23] J. S. Hong and M. J. Lancaster, *Microstrip Filters for RF/Microwave Applications*. New York, NY, USA: Wiley, 2001.
- [24] H. Wang, “Design and modeling of monolithic circuits Schottky diode on a GaAs substrate at millimeter and submillimeter wavelengths heterodyne receivers for multi-pixel and on board satellites dedicated to planetary astronomy,” Ph.D. dissertation, Dept. Astron. Astrophys., Univ. P&M Curie, Paris, France, 2009.
- [25] *Advanced Design System*, Agilent Technologies, USA, 2016.
- [26] CST, CST Microwave Studio, Germany, 2016.
- [27] J. V. Siles and J. Grajal, “Physics-based design and optimization of Schottky diode frequency multipliers for terahertz applications,” *IEEE Trans. Microw. Theory Techn.*, vol. 58, no. 7, pp. 1933–1942, Jul. 2010.



**Cheng Guo** was born in Chengdu, China, in 1990. He received the B.Eng. degree in communication engineering from Southwest Jiaotong University (Emei), Chengdu, China, in 2012, and the Ph.D. degree in radio physics from the University of Electronic Science and Technology of China (UESTC), Chengdu, China, in 2016.

From 2014 to 2016, he was a visiting Ph.D. student with the University of Birmingham and has been a Research Fellow with the same university since January 2017. His current research interests include 3-D printed passive microwave devices and Schottky diode based THz frequency multipliers and mixers.

Dr. Guo was the recipient of the IEEE MTT-S Tatsuo Itoh Award in 2017.



**Xiaobang Shang** (M’13) was born in Hubei, China, in 1986. He received the B.Eng. degree (First Class) in electronic and communication engineering from the University of Birmingham, Birmingham, U.K., in 2008, the B.Eng. degree in electronics and information engineering from the Huazhong University of Science and Technology (HUST), Wuhan, China, in 2008, and the Ph.D. degree in microwave engineering from the University of Birmingham, Edgbaston, Birmingham, U.K., in 2011. His doctoral research concerned micromachined terahertz circuits and

design of multiband filters.

He is currently a Senior Research Scientist with the National Physical Laboratory (NPL), Teddington, U.K. Prior to joining the NPL, he was a Research Fellow with the University of Birmingham. His current main research interests include microwave measurements, microwave filters and multiplexers, and micromachining techniques.

Dr. Shang was the recipient of the ARFTG Microwave Measurement Student Fellowship Award in 2009, the Tatsuo Itoh Award in 2017, and the Steve Evans-Pughe Prize (awarded by the ARMMS RF and Microwave Society) in 2017.



**Michael J. Lancaster** (SM’04) was born in the Keighley, Yorkshire, U.K., in 1958. He received the Graduate degree in physics and Ph.D. degree from Bath University, Bath, U.K., in 1980 and 1984, respectively. His doctoral research concerned nonlinear underwater acoustics.

After leaving Bath University, he joined the Surface Acoustic Wave (SAW) Group, Department of Engineering Science, Oxford University, as a Research Fellow, where his research concerned the design of new novel SAW devices, including RF filters and filter banks. In 1987, he became a Lecturer with the Department of Electronic and Electrical Engineering, University of Birmingham, lecturing in electromagnetic theory and microwave engineering. Shortly after he joined the department he began the study of the science and applications of high-temperature superconductors, working mainly at microwave frequencies. He became Head of the Emerging Device Technology Research Centre in 2000 and Head of the Department of Electronic, Electrical, and Computer Engineering in 2003. He has authored 2 books and more than 170 papers in refereed journals. His present personal research interests include microwave filters and antennas, as well as the high-frequency properties and applications of a number of novel and diverse materials.

Prof. Lancaster is Fellow of the IET and U.K. Institute of Physics. He is a Chartered Engineer and Chartered Physicist. He has served on the IEEE MTT-S IMS Technical Committee.



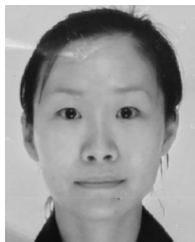
**Jun Xu** was born in China, in 1963. He received the B.S. and the M.S. degrees from the University of Electronic Science and Technology of China (UESTC), Chengdu, China, in 1984 and 1990, respectively.

In 1997, he became an Associate Professor with UESTC, and then became a Professor in 2000. He is currently the Head of the School of Physical Electronics, UESTC. His main research interests include microwave theory and technology, millimeter-wave hybrid integrated technology, millimeter-wave communication, radar radio frequency technology, as well as 3-D printing of passive microwave devices.



**Jeffrey Powell** received the B.Sc. and Ph.D. degrees from the University of Birmingham, Birmingham, U.K., in 1992 and 1995, respectively.

Following graduation he continued working at the University of Birmingham, where he investigated properties of ferroelectric and superconducting materials at microwave frequencies. From 2001 to 2010, he was a Principal Engineer with Qineti Q, where he performed many MMIC circuit, hybrid, and module designs for many applications from 2 to 110 GHz using a wide range of commercial and research-based circuit and packaging technologies. In 2010, he formed Skyarna Ltd, Halesowan, West Midlands, U.K., design consultancy that specializes in the design of leading edge circuits; including wideband high-efficiency amplifiers and active circuits to 300 GHz. He has contributed to more than 50 journal and conference publications and also 2 patent applications.



**Hui Wang** received the M.Sc. and Ph.D. degrees in astrophysics and space instrumentation from the University Pierre and Marie Curie, Paris, France, in 2005 and 2009, respectively.

She joined the Millimetre Wave Technology Group, STFC Rutherford Appleton Laboratory, in 2009. She is currently leading mixer device development within the group. Her current research interests include millimeter-wave and THz devices, primarily heterodyne frequency mixers and harmonic up-conversion multipliers, in support of earth observation and astronomy remote sounding experiments.



**Kai Parow-Souchon** received the M.Sc degree with a focus on CubeSat communication systems from RWTH Aachen University, Aachen, Germany, in 2014.

He then joined the Millimetre Wave Group, Rutherford Appleton Laboratory, Oxfordshire, U.K. He has primarily been involved with LNA design and packaging, as well as testing between 160 and 230 GHz for space-borne radiometers, as well as passive and quasi-optic components and systems.



**Manju Henry** received the Master's and Ph.D. degrees in electronic engineering from the Cochin University of Science and Technology, Kerala, India, in 1998 and 2002, respectively.

After her Ph.D., she did five years of post-doctoral studies with the Institute of High Frequency and Microwave Techniques (IHM), Karlsruhe Institute of Technology (formerly FZK), Karlsruhe, Germany, and with the University of Surrey, Surrey, U.K.

She joined the Millimetre Wave Technology Group, STFC Rutherford Appleton Laboratory, Oxfordshire, U.K., in 2007. After joining the group she undertook key technical and management roles with several EU/ESA programs. She is currently involved in a wide range of tasks that include millimeter-wave passive system design for atmospheric sounding and astronomy, active system development for meteorological remote sounding, and security imaging.



**Colin Viegas** received the B.E. degree in electronics and telecommunication engineering from the University of Mumbai, Mumbai, India, in 2009, and the M.Sc. and Ph.D. degrees from the University of Manchester, Manchester, U.K., in 2012 and 2017, respectively.

He is currently working with Teratech Components, where he is involved with the development of millimeter- and submillimeter-wave Schottky devices for local oscillators and mixers.



**Byron Alderman** received the M.Phys. degree in physics from the University of Warwick, Coventry, U.K., in 1998, and the Ph.D. degree from The University of Leeds, Leeds, U.K., in 2001.

Following graduation he joined the Millimetre Wave Technology Group, Rutherford Appleton Laboratory, Oxfordshire, U.K. He founded Teratech Components, in Oxfordshire, U.K., in 2010, where he is currently the CEO and a Principal Scientist with the Rutherford Appleton Laboratory. His research interests are in the field of room temperature heterodyne receiver technology for applications in remote sensing and astronomy at millimeter and submillimeter wavelengths.



**Peter G. Huggard** (SM'12) received B.A. (Mod) degree in experimental physics and Ph.D. degree from Trinity College, University of Dublin, Dublin, Trinity College, Ireland, in 1986 and 1991, respectively.

He then performed subsequent postdoctoral research with the University of Regensburg, Germany, and the University of Bath, Bath, U.K. Since 2000, he has been a member of the Millimetre Wave Technology Group, STFC Rutherford Appleton Laboratory, Oxfordshire, U.K. He is currently a U.K. Research Council's Individual Merit Fellow and the Deputy

Leader of the Millimetre Wave Technology Group. His interests include developing photonic sources and semiconductor diode based receivers for GHz and THz radiation, the characterization of frequency selective surfaces, and the calibration of millimeter-wave radiometers. He has contributed to more than 50 refereed journal papers and a similar number of conference proceedings.